Journal of Statistical Mechanics:
Theory and Experiment

**STOCHASTIC THERMODYNAMICS**

# An ordered set of power-efficiency trade-offs



Journal of Statistical Mechanics: Theory and Experiment
An IOP and SISSA journal

# An ordered set of power-efficiency trade-offs

**Hadrien Vroylandt**[1,2,4], **David Lacoste**[3] **and Gatien Verley**[1]

[1] Laboratoire de Physique Théorique (UMR8627), CNRS, Univ. Paris-Sud, Université Paris-Saclay, 91405 Orsay, France
[2] Department of Chemistry, Northwestern University, Evanston, IL 60208, United States of America
[3] Gulliver Laboratory, UMR CNRS 7083, PSL Research University, ESPCI, 10 rue Vauquelin, F-75231 Paris, France
E-mail: hadrien.vroylandt@northwestern.edu

Received 8 March 2019
Accepted for publication 22 March 2019
Published 13 May 2019

Online at stacks.iop.org/JSTAT/2019/054002
https://doi.org/10.1088/1742-5468/ab14d7

**Abstract.** In this paper, we derive a number of inequalities which express power-efficiency trade-offs that hold generally for thermodynamic machines operating in non-equilibrium stationary states. One of these inequalities concerns the output power, which is bounded by a quadratic function of the thermodynamic efficiency multiplied by a factor. Different factors can be obtained according to the level of knowledge one has about the underlying dynamics of the machine, they can depend for instance on the covariance of the input flux, the dynamical activity, or the non-equilibrium conductance.

**Keywords:** large deviations in non-equilibrium systems, stochastic thermodynamics, molecular motors, transport processes/heat transfer

[4] Author to whom any correspondence should be addressed.


1742-5468/19/054002+19$33.00

## Contents



## Introduction

In recent years, considerable efforts have been devoted to engineer new thermoelectric materials with the best possible efficiency [1] and to build small artificial stochastic engines mimicking molecular motors [2–4]. Clearly, in order to build the best possible machines, it is essential to develop a general understanding of the relationship between power, precision and dissipation [5]. What are the fundamental limits and design trade-offs involved in optimizing these three quantities?

This question is related to a major recent development in stochastic thermodynamics called the thermodynamic uncertainty relation, which is important because it goes beyond the usual formulation of the second law of thermodynamics [6]. This result establishes that the precision on a thermodynamic current in non-equilibrium stationary states comes with a minimal energetic cost [7, 8], where precision is quantified by the variance of the current and the energetic cost is measured by the dissipation. Applications of this thermodynamic uncertainty relation include among others, an

https://doi.org/10.1088/1742-5468/ab14d7


J. Stat. Mech. (2019) 054002

inference method to obtain the topology or the dissipation present in chemical networks [9–11], a characterization of Brownian clocks [12], bounds on the efficiency of molecular motors [13], design principles on non-equilibrium self-assembly [14] and much more.

For stochastic systems in contact with heat baths, a related result derived by Shiraishi *et al* [15] states that the square of the heat current between the system and heat bath is bounded by a system-dependent positive constant times the rate of entropy production. The Shiraishi *et al* result and the thermodynamic uncertainty relation both lead to similar power-efficiency trade-offs as far as the dependence on efficiency is concerned and the main difference between the two results lies in a system-dependent constant in factor of the function of the efficiency. Regardless of the precise value of this system-dependent positive constant, both results imply that the maximal efficiency of machines can only be realized at vanishing power output. The similarity between these two formulations of the power-efficiency trade-offs suggests that a general framework could exist, which presumably would include both formulations in a unifying way.

The search for such an unifying framework is motivating the present paper. In fact, a number of recent works are going in this direction: on one hand, the result of Shiraishi *et al* has been generalized to arbitrary currents besides the heat current, for non-thermal heat baths, and for dynamics with broken time-reversal symmetry but keeping the assumption of Langevin dynamics [6]. These authors obtained a general inequality based on the Cauchy–Schwartz inequality, according to which, the rate of entropy production is bounded from below by the square of any irreversible current. On the other hand, some of the limitations of the thermodynamic uncertainty relation have now been overcome, such as the assumption of steady states. Indeed, in [16] time-periodic machines have been studied in this context. These new results also follow from bounds on large deviation functions of a single current as in the original uncertainty relation, except that they no longer involve the entropy production, which is replaced by a different quantity. This quantity can be interpreted as the entropy production of the stationary dynamics that has the same mean current. Finally, another limitation of the uncertainty relation, the requirement of not breaking time-reversal dynamics, has been addressed in [17].

In this paper, we follow a somewhat different route as compared to these works, while still aiming at unifying power-efficiency trade-offs. Our approach is based on a concept we introduced in an earlier work, namely that of non-equilibrium conductance matrix [18]. This conductance matrix, relates physical currents to thermodynamic forces, just like the Onsager matrix, but generalizes it by being not limited to the near equilibrium regime. This new framework holds for systems operating in general non-equilibrium stationary states, i.e. arbitrarily far from equilibrium. By construction, this conductance matrix is a real, symmetric and semi-definite positive matrix, just like the Onsager matrix. One important difference with the Onsager matrix however, is that the coefficients of this matrix are not constants, but are functions of thermodynamic forces. Only near equilibrium, this dependence can be neglected in which case the non-equilibrium conductance matrix becomes identical with the Onsager matrix. This similarity with the Onsager matrix, allowed us to prove that the maximum thermodynamic efficiency achievable by a thermodynamic machine only depends of the so-called degree of coupling of the thermodynamic machine [18], thus generalizing an old result which was known for machines operating near equilibrium [19]. We also noted that

J. Stat. Mech. (2019) 054002

the macroscopic current-force relation does not lead to a unique conductance matrix, while a unique matrix can be built if the microscopic dynamics is known. To obtain an explicit matrix in this way, we considered a dynamics of Markov jump processes, and we obtained the non-equilibrium conductance matrix by extending a previously introduced large deviation formalism of stochastic currents [20].

In this paper, we derive a number of bounds using the method introduced in [18] and we make contact with the results of Dechant and Sasa [6] and of Shiraishi *et al* [15]. We find a hierarchy of inequalities in terms of either the conductance matrix, an activity matrix (which is a variant of the conductance matrix built from the transition frequencies instead of the local resistances), and the covariance matrix of the physical currents. This hierarchy of inequalities represents a generalization of the thermodynamic uncertainty relation that naturally leads to power-efficiency trade-offs. Finally, we illustrate these trade-offs using two examples of thermodynamic machines.

## 1. Power-efficiency trade-offs

### 1.1. Bounds on the output power

Let us focus on the simple case of a machine, in which a driving process, which we call the first process, drives another process, the second process. If we call $\sigma_1$ (resp. $\sigma_2$) the partial entropy production rate of the first (resp. second) process, we have $\sigma_1 \geqslant 0$ and $\sigma_2 \leqslant 0$. Let us then define the total entropy production as $\sigma = \sigma_1 + \sigma_2$, and the thermodynamic efficiency as $\eta = -\sigma_2/\sigma_1$. Using the definition of $\eta$ and the second law of thermodynamics $\sigma \geqslant 0$, we have $1 \geqslant \eta \geqslant 0$.

Let us also denote $F_X$ the affinity and $J_X$ the corresponding physical current of the process $X = 1, 2$ of the machine, then the partial entropy production rate $\sigma_X$ is simply $\sigma_X = F_X J_X$. As explained above, we relate the physical currents to the affinities by a generalization of the Onsager matrix, which we call the non-equilibrium conductance matrix $\boldsymbol{G}$, in such a way that $J_X = \sum_Y G_{X,Y} F_Y$ [18]. We then introduce a new parametrization of this matrix in terms of the degree of coupling $\xi = G_{12}/\sqrt{G_{11}G_{22}} \times \mathrm{sign}\,(F_1 F_2)$ and the relative intrinsic dissipation $\varphi = \sqrt{(G_{22}F_2^2)/(G_{22}F_1^2)}$. By expressing $-\sigma_2$ in terms of these parameters and optimizing with respect to them, we obtain the power-efficiency inequality:

$$-\sigma_2 \leqslant G_{11} F_1^2 \eta(1-\eta), \tag{1}$$

and alternatively using the component $G_{22}$ of the non-equilibrium conductance matrix

$$-\sigma_2 \leqslant G_{22} F_2^2 \frac{1-\eta}{\eta}. \tag{2}$$

An interesting and important consequence of these inequalities is that the output power (proportional to $-\sigma_2$) must vanish when the efficiency approaches its maximum value, i.e. when $\eta \to 1$, which corresponds for heat engines to the Carnot efficiency, unless both coefficients $G_{11}F_1^2$ or $G_{22}F_2^2$ diverge. The specific case where these coefficients diverge has been considered in [21 and 22].



J. Stat. Mech. (2019) 054002

An inequality of the type of equation (1) has been first derived in [15] for heat engines. In that work, the coefficient $G_{11}F_1^2$ was replaced by a model dependent coefficient $\bar{\Theta}$, for which an expression was provided for a system interacting with Langevin heat baths, in terms of the time average of the total kinetic energy of the engine, the temperature (of the baths), mass (of the engine) and damping constant (of the engine). A similar inequality has been derived in [13] by Pietzonka *et al* in the context of molecular motors based on the thermodynamic uncertainty relations [7, 8]. In their case, $G_{11}F_1^2$ is replaced by the variance of the input current.

### 1.2. Bounds on the input power

A similar calculation to that used to derive equations (1) and (2) also gives bounds on the input power $\sigma_1$ and on the total entropy production $\sigma$. Two types of bounds can be obtained by making the process one or two special. If one chooses to specialize to the process one, the input power $\sigma_1$ takes the following expression:

$$\sigma_1 = F_1^2 G_{11}\left(1+\xi\varphi\right). \tag{3}$$

By optimizing this expression with respect to $\varphi$ at constant $\xi$, one obtains a lower bound which only depends on the degree of coupling:

$$\sigma_1 \geqslant F_1^2 G_{11}\left(1-\xi^2\right). \tag{4}$$

As also done in the derivation of equations (1) and (2), in this optimization, one can treat $G_{11}$ as constant, because there are only two independent parameters in the conductance matrix, so they can be chosen to be $\varphi$ and $\xi$.

In order to obtain a different bound now in terms of the efficiency $\eta$ rather than the degree of coupling, one uses the expression of $\varphi$ as a function of $\eta$ and $\xi$ [18]:

$$\varphi^{\pm} = -\frac{\xi\left(\eta+1\right)}{2} \pm \frac{1}{2}\sqrt{(\eta+1)^2\xi^2 - 4\eta}, \tag{5}$$

which is then reported into equation (3). One obtains two functions of $\xi$, $\sigma_1^{\pm}(\xi)$, which are such that $\sigma_1^{+}(\xi) \geqslant \sigma_1^{-}(\xi)$. Since $\sigma_1^{+}(\xi)$ is a monotonously decreasing function of $\xi$, this function reaches its maximum at $\xi = -1$. Reporting this value into the expression of $\sigma_1^{+}$ leads to the upper bound

$$\sigma_1 \leqslant G_{11}F_1^2(1-\eta). \tag{6}$$

If we instead choose to make the second process special, one starts with

$$\sigma_1 = F_2^2 G_{22}\frac{1+\xi\varphi}{\varphi^2}. \tag{7}$$

Now, after reporting the expression of $\varphi^{\pm}$ into this $\sigma_1$, one obtains two solutions which are such that $\sigma_1^{+}(\xi) \leqslant \sigma_1^{-}(\xi)$. Then, the upper bound is obtained by reporting $\xi = -1$ into $\sigma_1^{-}$, which leads to

$$\sigma_1 \leqslant G_{22}F_2^2\frac{1-\eta}{\eta^2}. \tag{8}$$

https://doi.org/10.1088/1742-5468/ab14d7


J. Stat. Mech. (2019) 054002

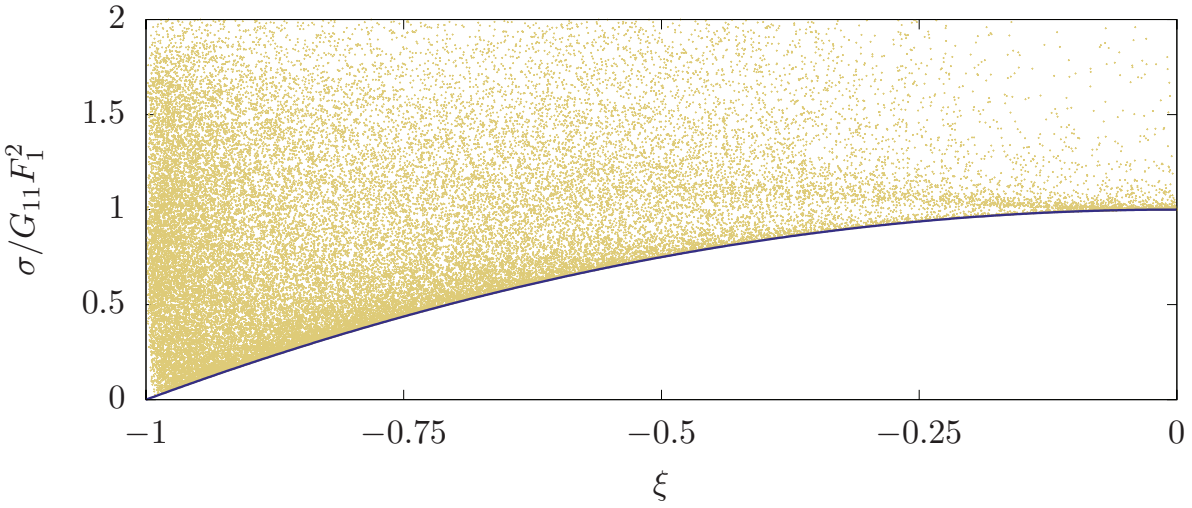


**Figure 1.** Total entropy production as function of the degree of coupling for the molecular motor model introduced in section 3.2. The violet solid line is the bound of equation (9). The kinetic parameters of the model are randomly chosen by multiplying the values used in figure 2(a) by $e^x$ with $x$ drawn uniformly within $[-2, 2]$, whereas the values of the affinity are uniformly drawn within $[-3, 1]$ for $f$ and $[3, 7]$ for $\Delta\mu$.

### 1.3. Bounds on the total entropy production

Similarly, the total entropy production can be expressed in terms of $\varphi$ and $\xi$ by choosing either the first or the second process as special. An optimization with respect to $\varphi$ at constant $\xi$ leads in the former case to the bound:

$$\sigma \geqslant F_1^2 G_{11} \left(1 - \xi^2\right), \tag{9}$$

and to

$$\sigma \geqslant F_2^2 G_{22} \left(1 - \xi^2\right), \tag{10}$$

in the later case. It is interesting to note that these lower bounds represent an improvement with respect to the second law, except at tight coupling when $\xi = -1$ where the inequalities (9) and (10) become the second law $\sigma \geqslant 0$. Similarly, for the partial entropy production, (4) represents an improvement with respect to the second law for the partial entropy production $\sigma_1 \geqslant 0$ except at tight coupling. Interestingly, in addition to these lower bounds, this framework also leads to upper bounds on the input power such as (6) and (8). In the limit where $\eta \to 1$, these upper bounds impose that the input power should vanish $\sigma_1 \to 0$ since $\sigma_1 \geqslant 0$. It is clear that this should be the case since we have already noted that in general $\sigma_2 \to 0$ as $\eta \to 1$, therefore given the definition of $\eta$, $\sigma_1 \to 0$ as $\eta \to 1$.

The improved bound on the total entropy production of (9) is tested in figure 1 for a stochastic model of a molecular motor which will be presented in details in section 3.2. The test consists in varying systematically kinetic parameters of the model and evaluating in each case the entropy production and the degree of coupling. The same



J. Stat. Mech. (2019) 054002

figure for the bound (10) presents similar features but is not presented. A related test also performed in the same way with this model checked that the maximum efficiency only depends on the degree of coupling [18].

## 2. Hierarchy of matrix inequalities

### 2.1. Conductance, activity and covariance matrices for Markov jump processes

We use a Markov jump process to model a mesoscopic machine with a finite number of states. The probability per unit time to jump from state $y$ to state $x$ is given by the rate matrix $\boldsymbol{k}$ of components $k_{(x,y)} \geqslant 0$. We call the couple of states $(x, y)$ an oriented edge when $k_{(x,y)} > 0$. We assume that if the jump from $y$ to $x$ is possible then the reverse jump also exists, i.e. $k_{(x,y)} > 0$ implies that $k_{(y,x)} > 0$. The stationary probability of $x$, denoted $\pi_x$, verifies by definition $\sum_y k_{(x,y)}\pi_y = 0$. The mean probability current along edge $(x, y)$ in the stationary state is

$$J_{(x,y)} \equiv k_{(x,y)}\pi_y - k_{(y,x)}\pi_x, \tag{11}$$

and the corresponding edge affinity writes

$$F_{(x,y)} \equiv \ln \frac{k_{(x,y)}\pi_y}{k_{(y,x)}\pi_x}. \tag{12}$$

We also introduce the physical matrix $\bar{\boldsymbol{\phi}}$ that connects the edge current to the physical current by

$$J_X = \sum_{(x,y)} \bar{\phi}_{X,(x,y)} J_{(x,y)}, \quad X = 1, 2. \tag{13}$$

From the mean probability currents and edge affinities, we define an edge conductance $\bar{G}_{(x,y)} \equiv J_{(x,y)}/F_{(x,y)}$ which is a diagonal matrix in the space of edges. In [18], we derived a unique expression of the non-equilibrium conductance matrix by combining edge resistances (inverse of edge conductances) in series, and cycle conductance in parallel, leading to

$$\boldsymbol{G} \equiv \bar{\boldsymbol{\phi}} \cdot \boldsymbol{\mathcal{C}} \cdot \left(\boldsymbol{\mathcal{C}}^{\mathrm{T}} \cdot \bar{\boldsymbol{G}}^{-1} \cdot \boldsymbol{\mathcal{C}}\right)^{-1} \cdot \boldsymbol{\mathcal{C}}^{\mathrm{T}} \cdot \bar{\boldsymbol{\phi}}^{\mathrm{T}}, \tag{14}$$

where $\boldsymbol{\mathcal{C}}$ is the cycle matrix whose columns represent fundamental cycles on the graph of the machine and lines correspond to edges on the graph [20, 23]. Each component of the matrix $\boldsymbol{\mathcal{C}}$ is 1 or $-1$ if the edge belongs to the cycle (with sign $+$ if the cycle and edge have the same orientation), and 0 otherwise.

In the study of non-equilibrium processes, the edge activity matrix $\bar{\boldsymbol{A}}$ of diagonal components

$$\bar{A}_{(x,y)} \equiv k_{(x,y)}\pi_y + k_{(y,x)}\pi_x, \tag{15}$$

is of fundamental importance [24–27]. In this equation, $\bar{A}_{(x,y)}$ represents the mean number of jumps (irrespective of the direction of the jumps) per unit time between states $x$



J. Stat. Mech. (2019) 054002

and $y$ in the stationary state. The edge activity is as important as the edge resistance for transport properties because if the machine almost never performs a transition along an edge (which means it has a low activity), this edge resistance should be high. This argument explains why the dynamical activity should matter not only for the thermodynamic uncertainty relations [28], but more generally for key properties of the machine such its output power or its efficiency. In exact parallel with the conductance matrix, we introduce the matrix of dynamical activity $\boldsymbol{A}$ as

$$\boldsymbol{A} \equiv \bar{\boldsymbol{\phi}} \cdot \boldsymbol{\mathcal{C}} \cdot \left( \boldsymbol{\mathcal{C}}^{\mathrm{T}} \cdot \bar{\boldsymbol{A}}^{-1} \cdot \boldsymbol{\mathcal{C}} \right)^{-1} \cdot \boldsymbol{\mathcal{C}}^{\mathrm{T}} \cdot \bar{\boldsymbol{\phi}}^{\mathrm{T}}, \tag{16}$$

where the edge activity appears instead of the edge conductance with respect to equation (14).

Finally, we define the covariance matrix $\boldsymbol{C}$ of physical currents

$$C_{XY} \equiv \lim_{t\to\infty} t \left[ \langle j_X j_Y \rangle - \langle j_X \rangle \langle j_Y \rangle \right], \tag{17}$$

where $j_X$ is the stochastic current for the driving process ($X = 1$) or the output current ($X = 2$). We denote by $\langle ... \rangle$ the mean value in the stationary state, i.e. $\langle j_X \rangle = J_X$. The covariance matrix characterizes the small fluctuations of currents around their average.

Close to equilibrium case, the fluctuations-dissipation theorem connects the fluctuations characterized by the matrix $\boldsymbol{C}$ and the Onsager response matrix that is linked to dissipation. Far from equilibrium, the thermodynamic uncertainty relation replaces the fluctuations-dissipation theorem. In our framework, this shows up as a hierarchy of inequalities for the matrices $\boldsymbol{G}$, $\boldsymbol{A}$ and $\boldsymbol{C}$, emphasizing the key role played by the dynamical activity in non-equilibrium systems.

### 2.2. From matrix inequalities to power-efficiency trade-offs

In order to compare the various matrices introduced above, it is useful to introduce among them the Loewner partial order [29]. Given two symmetric $n \times n$ matrices $\boldsymbol{V}$ and $\boldsymbol{W}$, we write $\boldsymbol{V} \geqslant \boldsymbol{W}$ when $\boldsymbol{V} - \boldsymbol{W}$ is a positive semi-definite matrix, which also means that

$$\boldsymbol{V} \geqslant \boldsymbol{W} \Leftrightarrow \left( \forall \boldsymbol{x} \in \mathbb{R}^n, \quad \boldsymbol{x}^{\mathrm{T}} \cdot \boldsymbol{V} \cdot \boldsymbol{x} \geqslant \boldsymbol{x}^{\mathrm{T}} \cdot \boldsymbol{W} \cdot \boldsymbol{x} \right). \tag{18}$$

With this definition, we derive in appendix A the following matrix inequalities using a large deviation framework:

$$\boldsymbol{G} \leqslant \frac{\boldsymbol{A}}{2} \leqslant \frac{\boldsymbol{C}}{2}. \tag{19}$$

We view equation (19) as a fluctuation-activity-dissipation inequality. At equilibrium, the non-equilibrium conductance matrix becomes the Onsager matrix $\boldsymbol{L}$, and the two inequalities above saturate because $\boldsymbol{L} = \boldsymbol{A}/2 = \boldsymbol{C}/2$.

Using equations (18) and (19) and chosing $\boldsymbol{x} = (1, 0)^{\mathrm{T}}$, we find

$$G_{11} \leqslant \frac{1}{2} A_{11} \leqslant \frac{1}{2} C_{11}. \tag{20}$$



J. Stat. Mech. (2019) 054002

After multiplying these inequalities by $F_1^2$, we obtain $G_{11}F_1^2 \leqslant A_{11}F_1^2/2 \leqslant C_{11}F_1^2/2$. Then, three different bounds on the output entropy production rate follows from equation (1), in terms of the first coefficients of the non-equilibrium conductance, of the activity or of the current covariance matrices:

$$-\sigma_2 \leqslant G_{11}F_1^2\eta(1-\eta) \leqslant \frac{A_{11}}{2}F_1^2\eta(1-\eta) \leqslant \frac{C_{11}}{2}F_1^2\eta(1-\eta). \tag{21}$$

Note that equation (21) contains the trade-off derived by Pietzonka *et al* [13].

In contrast to that, the trade-offs obtained by Sasa–Dechant [6], see also Shiraishi *et al* [15] take the following form for Markovian dynamics on a graph:

$$-\sigma_2 \leqslant \frac{A_{11}}{2}F_1^2\eta(1-\eta) \leqslant \frac{1}{2}A_\phi F_1^2\eta(1-\eta), \tag{22}$$

where $A_\phi = \sum_{(x,y)} \bar{\phi}^2_{1,(x,y)}A_{(x,y)}$ is an average dynamical activity with respect to the same function $\phi_{1,(x,y)}$ introduced in equation (13) to relate physical and edge currents. Despite a common origin among all these trade-offs (see appendix B for details), we note that there is no general ordering between $A_\phi$ in equation (22) and the term proportional to $C_{11}$ in equation (21).

We conclude this section by emphasizing that we focused on the bounds following from equation (1) combined with the matrix inequalities of equation (19) or with the bound for $A_{11}$ following from Cauchy–Schwartz inequality, but it is straightforward to obtain similar upper bounds for the other inequalities of section 1.

## 3. Illustrative examples

In this section, we illustrate our power-efficiency bounds using two simple models of thermodynamic autonomous machines studied in [18]: a unicyclic thermal engine and an isothermal molecular motor that has several cycles. We first describe these two models and then discuss our main results.

### 3.1. Unicyclic thermal engine

We start with the unicyclic heat-to-heat converter with three states $a, b$ and $c$ of energy $E_a, E_b, E_c$. Each transition is promoted by a different heat reservoir at inverse temperature $\beta_1, \beta_2, \beta_3$. We take the Boltzmann constant $k_\mathrm{B} = 1$, and set the energy scale by taking $\beta_3 = 1$. The transition rates are

$$\begin{aligned} k_{(b,a)} &= \Gamma \mathrm{e}^{-\frac{\beta_1}{2}(E_b-E_a)}, \quad k_{(a,b)} = \Gamma \mathrm{e}^{-\frac{\beta_1}{2}(E_a-E_b)}, \\ k_{(c,b)} &= \Gamma \mathrm{e}^{-\frac{\beta_2}{2}(E_c-E_b)}, \quad k_{(b,c)} = \Gamma \mathrm{e}^{-\frac{\beta_2}{2}(E_b-E_c)}, \\ k_{(a,c)} &= \Gamma \mathrm{e}^{-\frac{\beta_3}{2}(E_a-E_c)}, \quad k_{(c,a)} = \Gamma \mathrm{e}^{-\frac{\beta_3}{2}(E_c-E_a)}, \end{aligned} \tag{23}$$

where $\Gamma$ is the coupling constant to the heat reservoirs which defines the unit of time and which we take to be $\Gamma = 1$. Since the converter is coupled to three heat reservoirs, the



J. Stat. Mech. (2019) 054002

total entropy production rate writes $\sigma = -\beta_1 J_1 - \beta_2 J_2 - \beta_3 J_3$, where $J_i$ denotes the heat flux from the heat reservoir $i$ to the system. Using energy conservation $J_1 + J_2 + J_3 = 0$, we simplify the total entropy production rate as $\sigma = (\beta_3 - \beta_1)J_1 + (\beta_3 - \beta_2)J_2$. In agreement with section 1, we consider as driving process the heat flow $J_1$ and as output process the heat flow $J_2$. Without loss of generality, we assume the following inequalities for the reservoir's temperatures $\beta_3 > \beta_1$ and $\beta_3 > \beta_2$ and for the energy levels $E_b > E_c > E_a$. Under these conditions, the driving and output currents are such that $J_1 > 0$ and $J_2 < 0$: the system operates as a machine that transfers heat from a cold to a hot reservoir using the thermodynamic force generated by the transfer of heat from a hot to a cold reservoir. The partial entropy production rates and physical affinities are then

$$\begin{aligned} \sigma_1 &= (\beta_3 - \beta_1)J_1, \quad F_1 = (\beta_3 - \beta_1) \\ \sigma_2 &= (\beta_3 - \beta_1)J_2, \quad F_2 = (\beta_3 - \beta_2). \end{aligned} \tag{24}$$

We emphasize that this model is unicyclic and hence satisfies the tight coupling condition. Therefore, the currents $J_1$ and $J_2$ are proportional to each other and at stalling, i.e. when $J_2 = 0$, the heat to heat converter works reversibly and does not produce entropy.

### 3.2. Molecular motor model

Our second example is a discrete model of a molecular motor [30, 31]. The motor has only two internal states and evolves on a linear discrete lattice by consuming Adenosine triphosphate (ATP) molecules. The position of the motor is given by two variables: the position $n$ on the lattice and $y$ is the number of ATP consumed. The even and odd sites are denoted by $a$ and $b$, respectively. Note that the lattice of $a$ and $b$ sites extends indefinitely in both directions along the $n$ and $y$ axis; for the spatial direction $n$, the lattice step defines the unit length. There are two physical forces acting on the motor, a chemical force controlled by the chemical potential difference of the hydrolysis reaction of ATP, $\Delta\mu$ and a mechanical force $f$ applied directly on the motor. The whole system is in contact with a heat bath, and we choose to express all quantities in units of $k_{\mathrm{B}}T$. Equilibrium corresponds to the vanishing of the two currents, namely the mechanical current $\bar{v}$ which is the average velocity of the motor on the lattice, and the chemical current $r$, which is its average rate of ATP consumption. Since the system operates cyclically, the change of internal energy in a cycle is zero and the first law takes the form $q + r\Delta\mu + f\bar{v} = 0$ where $q$ is the heat flow coming from the heat bath, $r\Delta\mu$ represents the chemical work and $f\bar{v}$ represents the mechanical work; all quantities are evaluated in a cycle. Under these conditions, the second law takes the form $\sigma = -q$, and the entropy production rate takes the following form:

$$\sigma = f\bar{v} + r\Delta\mu. \tag{25}$$

In the normal operation of the motor, chemical energy is converted into mechanical energy, which means that the driving process (1) is the chemical one and the output process (2) the mechanical one in agreement with the convention made in this paper. Thus, the two partial entropy production rates should be $\sigma_1 = r\Delta\mu$, with the chemical affinity $F_1 = \Delta\mu$ and $\sigma_2 = f\bar{v}$, with mechanical affinity $F_2 = f$.



J. Stat. Mech. (2019) 054002

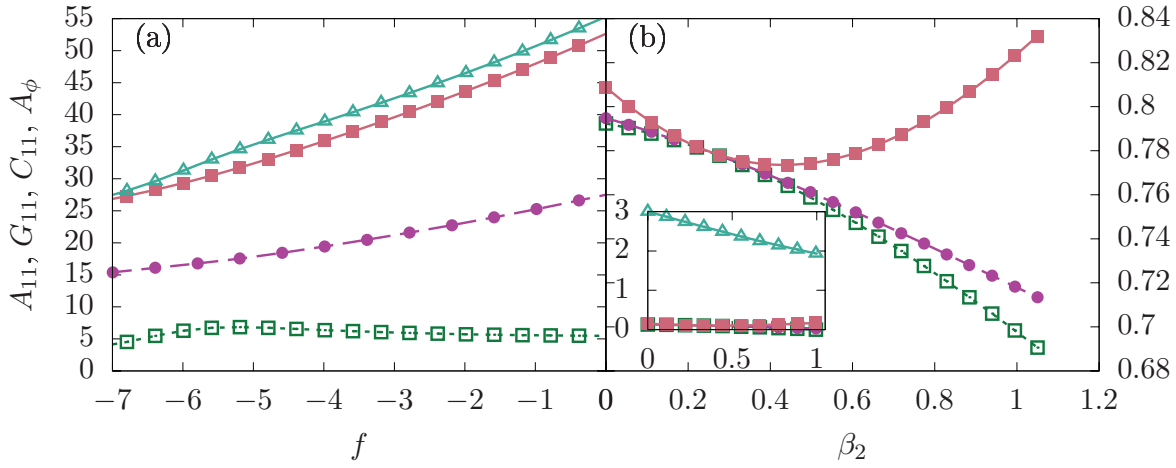


**Figure 2.** Trade-off coefficients versus the force acting on the molecular motor in (a) or versus the inverse temperature $\beta_2$ for the unicyclic thermal engine in (b). The green empty squares are the coefficient $G_{11}$ of the conductance matrix, the violet circles are the coefficient $A_{11}$ of the activity matrix, the coefficient $C_{11}$ of the covariance matrix is shown with the red full squares and the input power activity $A_\phi$ is the blue empty triangles. Insert: a larger view of the main figure. For figure (a), the parameters are $\Delta\mu = 20.0$, $\alpha = 0.57$, $\alpha' = 1.3.10^{-6}$, $\omega = 3.5$, $\omega' = 108.15$ $\epsilon = 10.81$, $\theta_a^+ = 0.25$, $\theta_a^- = 1.83$, $\theta_b^+ = 0.08$, $\theta_b^- = -0.16$. For (b), they are $\beta_1 = 0.5$, $\beta_3 = 1$, $\Gamma = 1$, $E_a = 1$, $E_b = 4$ and $E_c = 2$.

### 3.3. Discussion

In order to illustrate the inequalities (19), we plot the $(1,1)$ coefficients of the three matrices $\boldsymbol{G}$, $\boldsymbol{A}/2$, $\boldsymbol{C}/2$ and the dynamical activity parameter $A_\phi$ in figure 2 for the unicyclic engine and the molecular motor as function of the output affinities for both machines. We confirm the order between the different coefficients predicted by equations (19)–(22).

In the chosen conditions, only the unicyclic engine can approach equilibrium, it does so around $\beta_2 = 0.3$. At this point, all three coefficients converge towards the same value.

On figure 3, we plot the four studied power-efficiency trade-offs. We confirm again the order among the four trade-offs. It can be also observed that in the case of the tight coupling machine, the inequality (1) becomes an equality [18].

It is interesting at this point to observe that the quality of the various bounds seems to be related to the level of information available about the system. Indeed, the tightest bound is the one obtained from the non-equilibrium conductance matrix, which is built using the knowledge of the microscopic dynamics of the system. The bound obtained from the dynamical activity is less tight, but it also requires less information since only time symmetric observables of the microscopic dynamics are used. The bounds deduced from the covariance matrix are the loosest bounds, and they indeed require the least information, since only information on macroscopic physical currents is needed instead of the more detailed stochastic dynamics of edge currents.

J. Stat. Mech. (2019) 054002

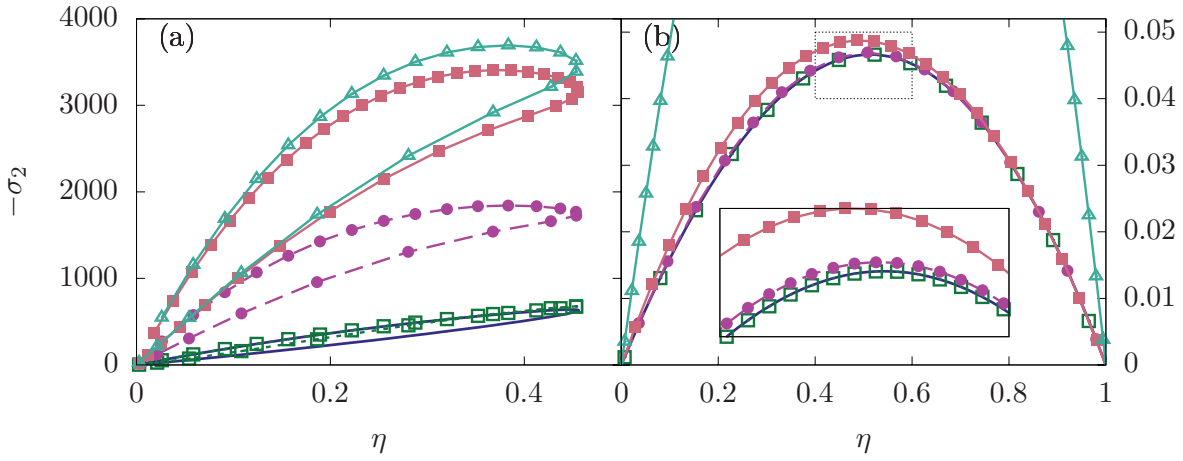


**Figure 3.** Output entropy production rate as a function of the thermodynamic efficiency for the molecular motor (a) or the unicyclic thermal engine (b). The solid line represents the output entropy production and the symbols represent the different power-efficiency trade-offs derived from the coefficients represented in figure 2 (with the same color code and shape). Inset: zoom in the region of the maximum power. Parameters are the same as in figure 2.

## 4. Conclusion

In this work, we have extended our previous framework on the conductance matrix for general thermodynamic machines operating in a non-equilibrium steady state arbitrarily far from equilibrium. By parametrizing this conductance matrix in terms of the degree of coupling, we obtain various bounds for the input and output power and for the total entropy production. It is easy to see that the bounds on the total or partial entropy production go beyond the second law of thermodynamics.

While these bounds can be proven generally, they involve a constant factor, a coefficient of the conductance matrix, which is in general unknown. To make progress, we choose a discrete Markov jump process for the microscopic dynamics, which allows to calculate explicitly important matrices for this problem, such as the conductance matrix, the activity matrix and the covariance matrix. We show that these matrices are ordered according to Loewner partial order, and that these matrix inequalities lead to an ordered set of power-efficiency trade-offs.

Our formulation includes a number of already known results such as the power-efficiency trade-off derived by Pietzonka and Seifert or the inequality previously obtained by Dechant and Sasa for Langevin systems. We obtain a hierarchy of power-efficiency trade-offs, with an order that depends primarily on the level of knowledge of the microscopic dynamics. The tightest bound is obtained when the maximum of information is available on the microscopic dynamics, while more loose bounds are obtained when only coarse-grained information is available.

The present work applies to stationary machines but not to periodically driven ones [32, 33]. We have also not considered systems with broken time-reversal symmetry [34] for which extensions of this framework could be carried out. We hope to address some of these extensions in future work.

J. Stat. Mech. (2019) 054002

## Appendix A. Derivation of the matrix inequalities

Let us consider in a stochastic description of the machine, a long trajectory of duration $T$, and $x(t)$ the label of the state occupied at time $t$. The empirical density is defined as the fraction of time a given trajectory spends in state $y$ as

$$p_y = \frac{1}{T}\int_0^T \mathrm{d}t\delta_{x(t),y}. \tag{A.1}$$

In the long time limit, $p_y$ tends to $\pi_y$ which is the stationary probability distribution. Furthermore, we denote the empirical edge current associated to the net number of transitions from $y$ to $x$ per unit time during a trajectory of duration $T$ by $j_{(x,y)}$, with

$$j_{(x,y)} = \frac{1}{T}\int_0^T \mathrm{d}t\left(\delta_{x(t^-),y}\delta_{x(t^+),x} - \delta_{x(t^+),y}\delta_{x(t^-),x}\right), \tag{A.2}$$

where $x(t^\pm)$ denotes the configuration immediately before or after time $t$. In the long time limit, $j_{(x,y)}$ tends to $J_{(x,y)}$, which is the steady state current. Beside these two currents, let us introduce the current $j^p_{(x,y)}$ that represents the expected edge current given the empirical density $\boldsymbol{p}$ and the edge rates

$$j^p_{(x,y)} = k_{(x,y)}p_y - k_{(y,x)}p_x. \tag{A.3}$$

Finally, we denote by $g^p_{(x,y)}$ the edge rates given $\boldsymbol{p}$ that represents the pairwise geometric average on direction of each transition rate

$$g^p_{(x,y)} = 2\sqrt{k_{(x,y)}k_{(y,x)}p_y p_x}. \tag{A.4}$$

The probability distribution $P(\{p_x\},\{j_{(x,y)}\})$ of the empirical density and edge currents obeys at large time $T$ a large deviation principle yielding

$$P(\{p_x\},\{j_{(x,y)}\}) \simeq \mathrm{e}^{-TI(\{p_x\},\{j_{(x,y)}\})}, \tag{A.5}$$

where $I(\{p_x\},\{j_{(x,y)}\})$ is a large deviation function (LDF) [35]. This LDF provides the rate at which decays with time the probability that empirical densities and edge currents remain different from their steady state values. This level of description is called the level 2.5 in the literature. The LDF at that level for Markov jump processes has an explicit form [10]:

$$\begin{aligned} I_{2.5}(\{p_x\},\{j_{(x,y)}\}) = &\sum_{(x,y)} j_{(x,y)}\mathrm{arcsinh}\left(\frac{j_{(x,y)}}{g^p_{(x,y)}}\right) - j_{(x,y)}\mathrm{arcsinh}\left(\frac{j^p_{(x,y)}}{g^p_{(x,y)}}\right) \\ &+ \sqrt{{j^p_{(x,y)}}^2 + {g^p_{(x,y)}}^2} - \sqrt{j^2_{(x,y)} + {g^p_{(x,y)}}^2}. \end{aligned} \tag{A.6}$$

To make useful predictions based on this LDF one must coarse-grain edge currents into physical currents [36], using that the latter are linearly related to the formers. Hence, the LDF for physical currents is obtained from equation (A.6) by the following contraction:



J. Stat. Mech. (2019) 054002

$$I(\boldsymbol{j}) = \min_{\{p_x\},\{..\}} I_{2.5}(\{p_x\},\{j_{(x,y)}\}), \tag{A.7}$$

where $\{..\}$ denotes here (and in the following) the minimum over edge currents $\{j_{(x,y)}\}$ that corresponds to the physical current $\boldsymbol{j}$ and respect the stationary condition

$$\forall x, \quad \sum_y (j_{(x,y)} - j_{(y,x)}) = 0. \tag{A.8}$$

A first bound follows from equation (A.7), once the empirical density $\{p_x\}$ is approximated by the stationary probability $\{\pi_x\}$, namely:

$$I(\boldsymbol{j}) \leqslant \min_{\{..\}} I_{2.5}(\{\pi_x\},\{j_{(x,y)}\}). \tag{A.9}$$

By performing a Taylor expansion of $I_{2.5}(\{\pi_x\},\{j_{(x,y)}\})$ around $j_{(x,y)} \simeq J_{(x,y)}$ at second order, one obtains an approximated function which we call $I_{\rm loc}(\{\pi_x\},\{j_{(x,y)}\})$, with

$$I_{\rm loc}(\{\pi_x\},\{j_{(x,y)}\}) = \sum_{(x,y)} \frac{(j_{(x,y)} - J_{(x,y)})^2}{2\sqrt{J_{(x,y)}^2 + g_{(x,y)}^{\pi\,2}}} = \sum_{(x,y)} \frac{(j_{(x,y)} - J_{(x,y)})^2}{2\bar{A}_{(x,y)}}. \tag{A.10}$$

Therefore, combining equations (A.9) and (A.10) leads to the local bound on current LDF

$$I(\boldsymbol{j}) \leqslant \min_{\{..\}} I_{2.5}(\{\pi_x\},\{j_{(x,y)}\}) \simeq \min_{\{..\}} I_{\rm loc}(\{\pi_x\},\{j_{(x,y)}\}). \tag{A.11}$$

We emphasize that the equation (A.11) is a local bound in the sense that it is valid only up to the second order of the Taylor expansion. As shown in [10], a closely related bound denoted $I_{\rm quad}$ leads this time to a global bound, namely $I_{2.5}(\{\pi_x\},\{j_{(x,y)}\}) \leqslant I_{\rm quad}(\{\pi_x\},\{j_{(x,y)}\})$, with

$$I_{\rm quad}(\{\pi_x\},\{j_{(x,y)}\}) = \frac{1}{4}\sum_{(x,y)} (j(x,y) - J_{(x,y)})^2 \frac{\sigma^\pi_{(x,y)}}{J^2_{(x,y)}}. \tag{A.12}$$

In this equation, $\sigma^\pi_{(x,y)}$ is the steady state entropy production rate associated to the transitions from $y$ to $x$ defined by

$$\sigma^\pi_{(x,y)} = (k_{(x,y)}\pi_y - k_{(y,x)}\pi_x)\ln\frac{k_{(x,y)}\pi_y}{k_{(y,x)}\pi_x}. \tag{A.13}$$

Now, using the relation $\sigma^\pi_{(x,y)} = J_{(x,y)}F_{(x,y)}$ and the definition $\bar{R}_{(x,y)} = F_{(x,y)}/J_{(x,y)}$, one can write $I_{\rm quad}$ as

$$I_{\rm quad}(\{\pi_x\},\{j_{(x,y)}\}) = \frac{1}{4}\sum_{(x,y)} (j(x,y) - J_{(x,y)})^2 \bar{R}_{(x,y)}. \tag{A.14}$$

Further, using the general inequality $(a-b)\ln(a/b) \geqslant 2(a-b)^2/(a+b)$, one deduces first that $\sigma^\pi_{(x,y)} \geqslant 2J^2_{(x,y)}/\bar{A}_{(x,y)}$ and then using equation (A.12) that

$$I_{\rm loc}(\{\pi_x\},\{j_{(x,y)}\}) \leqslant I_{\rm quad}(\{\pi_x\},\{j_{(x,y)}\}). \tag{A.15}$$



J. Stat. Mech. (2019) 054002

Using equations (A.7), (A.11) and (A.15), we obtain in the end:

$$I(\boldsymbol{j}) \leqslant \min_{\{..\}} I_{\mathrm{loc}}(\{\pi_x\}, \{j_{(x,y)}\}) \leqslant \min_{\{..\}} I_{\mathrm{quad}}(\{\pi_x\}, \{j_{(x,y)}\}). \tag{A.16}$$

Since we are now minimizing quadratic functions, we can find the minimizer exactly as in [18]:

$$I_{\mathrm{loc}}(\boldsymbol{j}) = \min_{\{..\}} I_{\mathrm{loc}}(\{\pi_x\}, \{j_{(x,y)}\}) = \frac{1}{2}(\boldsymbol{j}-\boldsymbol{J})^{\mathrm{T}} \cdot \boldsymbol{A}^{-1} \cdot (\boldsymbol{j}-\boldsymbol{J}) \tag{A.17}$$

$$I_{\mathrm{quad}}(\boldsymbol{j}) = \min_{\{..\}} I_{\mathrm{quad}}(\{\pi_x\}, \{j_{(x,y)}\}) = \frac{1}{4}(\boldsymbol{j}-\boldsymbol{J})^{\mathrm{T}} \cdot \boldsymbol{G}^{-1} \cdot (\boldsymbol{j}-\boldsymbol{J}) \tag{A.18}$$

with the expression of the matrix $\boldsymbol{G}$ and $\boldsymbol{A}$ being given by the equations (14) and (16). Since

$$I(\boldsymbol{J}) = I_{\mathrm{loc}}(\boldsymbol{J}) = I_{\mathrm{quad}}(\boldsymbol{J}) = 0 \quad \text{and} \quad \frac{\mathrm{d}I}{\mathrm{d}j}(\boldsymbol{J}) = \frac{\mathrm{d}I_{\mathrm{loc}}}{\mathrm{d}j}(\boldsymbol{J}) = \frac{\mathrm{d}I_{\mathrm{quad}}}{\mathrm{d}j}(\boldsymbol{J}) = 0, \tag{A.19}$$

the inequality (A.16) propagates to second order derivatives:

$$\boldsymbol{C}^{-1} \leqslant \boldsymbol{A}^{-1} \leqslant \frac{1}{2}\boldsymbol{G}^{-1}. \tag{A.20}$$

Using properties of semi-definite positive matrices [29] ends the proof of equation (19)

$$\boldsymbol{G} \leqslant \frac{\boldsymbol{A}}{2} \leqslant \frac{\boldsymbol{C}}{2}. \tag{A.21}$$

## Appendix B. Bound from an activity ansatz

The computation of conductance matrix and activity matrix in equations (A.17) and (A.18) requires the minimization of the bounds. Instead, we can rely on the use of an ansatz if we focus on only one current. Let us consider the stochastic current $j_1$ defined as a linear combination of edge currents

$$j_1 = \sum_{(x,y)} \bar{\phi}_{1,(x,y)} j_{(x,y)}. \tag{B.1}$$

To avoid the minimization in equation (A.16), we use an ansatz on edge current $\tilde{j}_{(x,y)}(j_1)$ that verifies

$$\sum_{(x,y)} \bar{\phi}_{1,(x,y)} \tilde{j}_{(x,y)}(j_1) = j_1, \tag{B.2}$$

and the stationary condition

$$\forall x, \quad \sum_{y} (\tilde{j}_{(x,y)}(j_1) - \tilde{j}_{(y,x)}(j_1)) = 0. \tag{B.3}$$

Following [8], the ansatz

$$\tilde{j}_{(x,y)}(j_1) = J_{(x,y)} \frac{j_1}{J_1} \tag{B.4}$$



J. Stat. Mech. (2019) 054002

works and can be used into equation (A.16) yielding

$$I(j_1) \leqslant I_{\rm loc}(\{\pi_x\}, \{\tilde{j}_{(x,y)}(j_1)\}) \leqslant I_{\rm quad}(\{\pi_x\}, \{\tilde{j}_{(x,y)}(j_1)\}). \tag{B.5}$$

The second derivative of this equation with respect to $j_1$ leads to

$$\frac{1}{{\rm Var}(j_1)} \leqslant \frac{\left(\sum_{(x,y)} \frac{J^2_{(x,y)}}{\bar{A}_{(x,y)}}\right)}{J_1^2} \leqslant \frac{\sigma}{2J_1^2}. \tag{B.6}$$

Due to Cauchy–Schwarz inequality, we have

$$J_1^2 = \left(\sum_{(x,y)} \bar{\phi}_{1,(x,y)} J_{(x,y)}\right)^2 \leqslant \left(\sum_{(x,y)} \bar{\phi}^2_{1,(x,y)} \bar{A}_{(x,y)}\right)\left(\sum_{(x,y)} \frac{J^2_{(x,y)}}{\bar{A}_{(x,y)}}\right), \tag{B.7}$$

where actually $\bar{A}_{(x,y)}$ could be arbitrary. Combining equations (B.6) and (B.7) gives then

$$\frac{J_1^2}{\sigma} \leqslant \frac{J_1^2}{2\left(\sum_{(x,y)} \frac{J^2_{(x,y)}}{\bar{A}_{(x,y)}}\right)} \leqslant \frac{1}{2}\left(\sum_{(x,y)} \bar{\phi}^2_{1,(x,y)} \bar{A}_{(x,y)}\right) = \frac{1}{2} A_\phi. \tag{B.8}$$

This equation is similar to the bound derived for Langevin systems in [6] (see equation (14) of that reference). It expresses a bound on the square of any current (here $J_1^2$) in terms of the total entropy production times a coefficient which depends on the activity. In diffusive systems, this activity may be expressed in terms of the diffusion coefficient of the system. We note that while the linear decomposition of equation (B.1) is general, we need to choose the specific function $\bar{\phi}_{1,(x,y)}$ introduced in equation (13) in order to apply the Cauchy–Schwartz inequality specifically to physical currents.

Notice that the term in the rhs of equation (B.8) could also be obtained by using as ansatz

$$\tilde{j}_{(x,y)}(j_1) = J_{(x,y)} + (j_1 - J_1)\frac{\bar{\phi}_{1,(x,y)}\bar{A}_{(x,y)}}{\sum_{(x,y)} \bar{\phi}^2_{1,(x,y)}\bar{A}_{(x,y)}}, \tag{B.9}$$

that respect the condition (B.2) but not the stationary condition (B.3). It happens that the ansatz (B.9) is the actual miminizer of $I_{\rm loc}(\{\pi_x\}, \{j_{(x,y)}\})$ under the constraint (B.2) but without considering the stationary condition. Therefore, pluging the ansatz of equation (B.9) inside $I_{\rm loc}(\{\pi_x\}, \{j_{(x,y)}\})$ leads to

$$I_{\rm loc}(\{\pi_x\}, \{\tilde{j}_{(x,y)}(j_1)\}) = \frac{(j_1 - J_1)^2}{2A_\phi} \leqslant \min_{\{..\}} I_{\rm loc}(\{\pi_x\}, \{j_{(x,y)}\}), \tag{B.10}$$

where as before the minimum of right hand side is carried over $\{j_{(x,y)}\}$ that corresponds to physical current $j_1$ and respect the stationary condition (B.3). Hence, using equation (A.17) and by deriving twice with respect to $j_1$, we obtain the inequality $A_{11} \leqslant A_\phi$ used in equation (22).



J. Stat. Mech. (2019) 054002

## Appendix C. Illustrative example: conductance and activity matrices

### C.1. Unicyclic heat-to-heat converter

Given the rates of the unicyclic heat-to-heat converter, we are able to determine the stationary probabilities $\pi_a$, $\pi_b$ and $\pi_c$ using for instance the spanning tree formula. We next compute the stationary cycle current $J_{c_1}$ and the mean activity on each edge $(i, j)$

$$\bar{A}_{(i,j)} = k_{(j,i)}\pi_i + k_{(i,j)}\pi_j. \tag{C.1}$$

That give us the conductance

$$\boldsymbol{G} = \frac{J_{c_1}}{F_{c_1}} \begin{pmatrix} (E_b - E_a)^2 & (E_c - E_b)(E_b - E_a) \\ (E_c - E_b)(E_b - E_a) & (E_c - E_a)^2 \end{pmatrix}, \tag{C.2}$$

and activity matrix

$$\boldsymbol{A} = \left( \frac{1}{\bar{A}_{(a,b)}} + \frac{1}{\bar{A}_{(b,c)}} + \frac{1}{\bar{A}_{(c,a)}} \right)^{-1} \begin{pmatrix} (E_b - E_a)^2 & (E_c - E_b)(E_b - E_a) \\ (E_c - E_b)(E_b - E_a) & (E_c - E_a)^2 \end{pmatrix}. \tag{C.3}$$

These expressions are used to draw figures 2(b) and 3(b).

### C.2. Molecular motor

The graph of this model includes four bidirectional edges connecting two states. For two of these edges, the transitions are passive and do not consume or produce ATP, but the other two are active. The eight transition rates associated to these four bidirectional edges are

$$\begin{aligned} \overrightarrow{\omega}_b^{-1} &= \alpha' \mathrm{e}^{\theta_b^+ f}, & \overrightarrow{\omega}_b^{0} &= \omega' \, \mathrm{e}^{\theta_b^+ f}, \\ \overleftarrow{\omega}_a^{1} &= \alpha' \mathrm{e}^{-\epsilon + \Delta\mu - \theta_a^- f}, & \overleftarrow{\omega}_a^{0} &= \omega' \, \mathrm{e}^{-\epsilon - \theta_a^- f}, \\ \overleftarrow{\omega}_b^{-1} &= \alpha \, \mathrm{e}^{-\theta_b^- f}, & \overleftarrow{\omega}_b^{0} &= \omega \, \mathrm{e}^{-\theta_b^- f}, \\ \overrightarrow{\omega}_a^{1} &= \alpha \, \mathrm{e}^{-\epsilon + \Delta\mu + \theta_a^+ f}, & \overrightarrow{\omega}_a^{0} &= \omega \, \mathrm{e}^{-\epsilon + \theta_a^+ f}, \end{aligned} \tag{C.4}$$

where we have kept the original notation of [30, 31]. In the above equations, $\theta_i^{\pm}$ represent load distribution factors that are arbitrary except that $\theta_a^+ + \theta_b^- + \theta_a^- + \theta_b^+ = 2$ [31]. Let us orientate all edges from state $a$ to $b$. Then, the four edge currents and affinities are

$$J_{(1)} = \pi_a \overleftarrow{\omega}_a^{1} - \pi_b \overrightarrow{\omega}_b^{-1}, \qquad F_{(1)} = \ln \frac{\overleftarrow{\omega}_a^{1} \pi_a}{\overrightarrow{\omega}_b^{-1} \pi_{\mathrm{B}}}, \tag{C.5}$$

$$J_{(2)} = \pi_a \overleftarrow{\omega}_a^{0} - \pi_b \overrightarrow{\omega}_b^{0}, \qquad F_{(2)} = \ln \frac{\overleftarrow{\omega}_a^{0} \pi_a}{\overrightarrow{\omega}_b^{0} \pi_{\mathrm{B}}}, \tag{C.6}$$

$$J_{(3)} = \pi_a \overrightarrow{\omega}_a^{0} - \pi_b \overleftarrow{\omega}_b^{0}, \qquad F_{(3)} = \ln \frac{\overrightarrow{\omega}_a^{0} \pi_a}{\overleftarrow{\omega}_b^{0} \pi_{\mathrm{B}}}, \tag{C.7}$$



J. Stat. Mech. (2019) 054002

$$J_{(4)} = \pi_a \overrightarrow{\omega_a}^1 - \pi_b \overleftarrow{\omega_b}^{-1}, \qquad F_{(4)} = \ln \frac{\overrightarrow{\omega_a}^1 \pi_a}{\overleftarrow{\omega_b}^{-1} \pi_{\mathrm{B}}}, \tag{C.8}$$

in terms of the stationary probabilities of states $a$ or $b$, denoted $\pi_a$ and $\pi_b$ respectively. For the explicit expressions of the probability currents in terms of the transition rates, we refer to [30, 31]. If one introduce the edge resistance matrix $\bar{R}_{(i)} = F_{(i)}/J_{(i)}$ with $i = 1, 2, 3$ and 4, the conductance matrix for this model writes

$$\boldsymbol{G} = \frac{1}{Z_G} \begin{pmatrix} (\bar{R}_{(1)} + \bar{R}_{(4)})(\bar{R}_{(3)} + \bar{R}_{(2)}) & 2(\bar{R}_{(4)}\bar{R}_{(2)} - \bar{R}_{(1)}\bar{R}_{(3)}) \\ 2(\bar{R}_{(4)}\bar{R}_{(2)} - \bar{R}_{(1)}\bar{R}_{(3)}) & 4(\bar{R}_{(1)} + \bar{R}_{(2)})(\bar{R}_{(3)} + \bar{R}_{(4)}) \end{pmatrix}, \tag{C.9}$$

with

$$Z_G = \bar{R}_{(1)}\bar{R}_{(4)}\bar{R}_{(3)} + \bar{R}_{(1)}\bar{R}_{(4)}\bar{R}_{(2)} + \bar{R}_{(1)}\bar{R}_{(3)}\bar{R}_{(2)} + \bar{R}_{(4)}\bar{R}_{(3)}\bar{R}_{(2)}. \tag{C.10}$$

The activity matrix is derived in a similar way and we obtain

$$\boldsymbol{A} = \frac{1}{Z_A} \begin{pmatrix} (\bar{A}_{(1)}^{-1} + \bar{A}_{(4)}^{-1})(\bar{A}_{(3)}^{-1} + \bar{A}_{(2)}^{-1}) & 2(\bar{A}_{(4)}^{-1}\bar{A}_{(2)}^{-1} - \bar{A}_{(1)}^{-1}\bar{A}_{(3)}^{-1}) \\ 2(\bar{A}_{(4)}^{-1}\bar{A}_{(2)}^{-1} - \bar{A}_{(1)}^{-1}\bar{A}_{(3)}^{-1}) & 4(\bar{A}_{(1)}^{-1} + \bar{A}_{(2)}^{-1})(\bar{A}_{(3)}^{-1} + \bar{A}_{(4)}^{-1}) \end{pmatrix}, \tag{C.11}$$

with

$$Z_A = \bar{A}_{(1)}^{-1}\bar{A}_{(4)}^{-1}\bar{A}_{(3)}^{-1} + \bar{A}_{(1)}^{-1}\bar{A}_{(4)}^{-1}\bar{A}_{(2)}^{-1} + \bar{A}_{(1)}^{-1}\bar{A}_{(3)}^{-1}\bar{A}_{(2)}^{-1} + \bar{A}_{(4)}^{-1}\bar{A}_{(3)}^{-1}\bar{A}_{(2)}^{-1} \tag{C.12}$$

and

$$A_{(1)} = \pi_a \overleftarrow{\omega_a}^1 + \pi_b \overrightarrow{\omega_b}^{-1}, \quad A_{(2)} = \pi_a \overleftarrow{\omega_a}^0 + \pi_b \overrightarrow{\omega_b}^0, \tag{C.13}$$

$$A_{(3)} = \pi_a \overrightarrow{\omega_a}^0 + \pi_b \overleftarrow{\omega_b}^0, \qquad A_{(4)} = \pi_a \overrightarrow{\omega_a}^1 + \pi_b \overleftarrow{\omega_b}^{-1}. \tag{C.14}$$

## References


[1] Benenti G, Casati G, Saito K and Whitney R S 2017 Fundamental aspects of steady-state conversion of heat to work at the nanoscale *Phys. Rep.* **694** 1–124

[2] Bustamante C, Liphardt J and Ritort F 2005 The nonequilibrium thermodynamics of small systems *Phys. Today* **58** 43–8

[3] Porto M, Urbakh M and Klafter J 2000 Atomic scale engines: cars and wheels *Phys. Rev. Lett.* **84** 6058–61

[4] Blickle V and Bechinger C 2012 Realization of a micrometre-sized stochastic heat engine *Nat. Phys.* **8** 143–6

[5] Pietzonka P and Seifert U 2018 Universal trade-off between power, efficiency, and constancy in steady-state heat engines *Phys. Rev. Lett.* **120** 190602

[6] Dechant A and Sasa S 2018 Entropic bounds on currents in Langevin systems *Phys. Rev.* E **97** 062101

[7] Barato A C and Seifert U 2015 Thermodynamic uncertainty relation for biomolecular processes *Phys. Rev. Lett.* **114** 158101

[8] Gingrich T R, Horowitz J M, Perunov N and England J L 2016 Dissipation bounds all steady-state current fluctuations *Phys. Rev. Lett.* **116** 120601

[9] Proesmans K, Peliti L and Lacoste D 2018 A case study of thermodynamic bounds for chemical kinetics *Chemical Kinetics Beyond the Textbook* (Singapore: World Scientific)

[10] Gingrich T R, Rotskoff G M and Horowitz J M 2017 Inferring dissipation from current fluctuations *J. Phys. A: Math. Gen.* **50** 184004

[11] Barato A C and Seifert U 2015 Universal bound on the Fano factor in enzyme kinetics *J. Phys. Chem.* B **119** 6555–61




J. Stat. Mech. (2019) 054002

[12] Barato A C and Seifert U 2016 Cost and precision of Brownian clocks *Phys. Rev.* X **6** 041053
[13] Pietzonka P, Barato A C and Seifert U 2016 Universal bound on the efficiency of molecular motors *J. Stat. Mech.* 124004
[14] Nguyen M and Vaikuntanathan S 2016 Design principles for nonequilibrium self-assembly *Proc. Natl Acad. Sci.* **113** 14231–6
[15] Shiraishi N, Saito K and Tasaki H 2016 Universal trade-off relation between power and efficiency for heat engines *Phys. Rev. Lett.* **117** 190601
[16] Barato A C, Chetrite R, Faggionato A and Gabrielli D 2018 Bounds on current fluctuations in periodically driven systems *New J. Phys.* **20** 103023
[17] Macieszczak K, Brandner K and Garrahan J P 2018 Unified thermodynamic uncertainty relations in linear response *Phys. Rev. Lett.* **121** 130601
[18] Vroylandt H, Lacoste D and Verley G 2018 Degree of coupling and efficiency of energy converters far-from-equilibrium *J. Stat. Mech.* 023205
[19] Caplan S R 1966 The degree of coupling and its relation to efficiency of energy conversion in multiple-flow systems *J. Theor. Biol.* **10** 209–35
[20] Polettini M, Lazarescu A and Esposito M 2016 Tightening the uncertainty principle for stochastic currents *Phys. Rev.* E **94** 052104
[21] Polettini M and Esposito M 2017 Carnot efficiency at divergent power output *Europhys. Lett.* **118** 40003
[22] Apertet Y 2017 Comment on 'Carnot efficiency at divergent power output' by Polettini Matteo and Esposito Massimiliano *Europhys. Lett.* **120** 60002
[23] Polettini M, Bulnes-Cuetara G and Esposito M 2016 Conservation laws and symmetries in stochastic thermodynamics *Phys. Rev.* E **94** 052117
[24] Maes C, Netočný K and Wynants B 2008 On and beyond entropy production: the case of Markov jump processes *Markov Process. Relat. Fields* **14** 445–64
[25] Baiesi M, Maes C and Wynants B 2009 Fluctuations and response of nonequilibrium states *Phys. Rev. Lett.* **103** 010602
[26] Basu U, Kruger M, Lazarescu A and Maes C 2015 Frenetic aspects of second order response *Phys. Chem. Chem. Phys.* **17** 6653–66
[27] Wynants B 2010 Structures of nonequilibrium fluctuations: dissipation and activity *PhD Thesis* Universiteit K.U. Leuven
[28] Di Terlizzi I and Baiesi M 2019 Kinetic uncertainty relation *J. Phys. A: Math. Theor.* **52** 02LT03
[29] Horn R A and Johnson C R 1985 *Matrix Analysis* (Cambridge: Cambridge University Press)
[30] Lau A W C, Lacoste D and Mallick K 2007 Nonequilibrium fluctuations and mechanochemical couplings of a molecular motor *Phys. Rev. Lett.* **99** 158102
[31] Lacoste D, Lau A W C and Mallick K 2008 Fluctuation theorem and large deviation function for a solvable model of a molecular motor *Phys. Rev.* E **78** 011915
[32] Koyuk T, Seifert U and Pietzonka P 2019 A generalization of the thermodynamic uncertainty relation to periodically driven systems *J. Phys. A: Math. Theor.* **52** 02LT02
[33] Barato A C, Chetrite R, Faggionato A and Gabrielli D 2018 A unifying picture of generalized thermodynamic uncertainty relations (arXiv:1810.11894)
[34] Proesmans K and Horowitz J 2019 Hysteretic thermodynamic uncertainty relation for systems with broken time-reversal symmetry (arXiv:1902.07008)
[35] Touchette H 2009 The large deviation approach to statistical mechanics *Phys. Rep.* **478** 1–69
[36] Verley G 2016 Nonequilibrium thermodynamic potentials for continuous-time Markov chains *Phys. Rev.* E **93** 012111

J. Stat. Mech. (2019) 054002